JOURNAL OF MATERIALS SCIENCE **34** (1999) 629–636

Crack propagation behavior of cermets and cemented carbides under repeated thermal shocks by the improved quench test

SOTOMI ISHIHARA, TAKAHITO GOSHIMA, KOJI NOMURA, TAKASHI YOSHIMOTO
Department of Mechanical Engineering, Faculty of Engineering, Toyama University, Toyama 930-8555, Japan
E-mail: ishi@eng.Toyama-u.ac.jp

In this study, an improved quench testing method for thermal shock resistance has been proposed. Repeated thermal shock tests were performed on cemented carbides to show the advantages of the new proposed method that would enable us to estimate an intrinsic relationship between the crack propagation rate and the stress intensity factor under repeated thermal shocks. The cyclic thermal fatigue crack propagation behavior and fracture toughness values were shown to be independent of the specimen heights and the cooling media employed. We then evaluated the thermal crack propagation behavior for cermets and cemented carbides by using this method, and discussed the differences between both materials in the crack growth behavior on the basis of their microstructures.

1. Introduction

Recently, cermets have been often used as a cutting tool material, to fill the increasing need for efficient and high-speed cutting. Cermets have several superior features, such as high resistance to wear and good capability for dressing surfaces of the works. In high-feed and intermittent cutting, many cracks are initiated due to repeated thermal or mechanical shocks. Therefore, to develop good cutting tools, it is necessary to clarify the repeated thermal shock behavior of the cutting materials [1]. Nevertheless, very few studies on thermal shock behavior have been done for cemented carbides and cermets, cutting tools, as compared with many kinds of ceramics.

Quench tests [2–14] have been employed to evaluate the thermal shock resistance of the materials tested. In these tests, the critical temperatures T_c at which bending strength after thermal shock drops abruptly due to initiations of thermal cracks are used as a scale for thermal shock resistance. The quench test has the advantage of being easily conducted, but has the disadvantage of an absence of the physical meaning for the parameter T_c used. For example, changes in the specimen sizes, specimen shapes and cooling medium yield different values of T_c, even if the same material is tested. Therefore it is difficult to obtain reliable T_c values, and also determine the quantitative relationship between subcritical crack growth rate and stress intensity factor under repeated thermal shock tests. Thermal boundary conditions between the specimen surface and the cooling media change in a complex way, and cannot be predicted or perhaps "explained" [15–16].

In this study, an improved quench method for a thermal shock experiment has been proposed. First, repeated thermal shock tests by the new method were performed on cemented carbides to confirm that the cyclic thermal fatigue crack propagation behavior and fracture toughness values are independent of the specimen heights and cooling medium with two different coefficients of kinematic viscosities. Then by using this novel method, we evaluated the crack propagation behavior and fracture toughness values for both cermets and cemented carbides, and discussed the differences in the crack growth behavior between both materials on the basis of their microstructures.

2. Specimens and experimental procedures

2.1. Specimens

The materials tested were cermets and cemented carbides with 8.5 μm WC grain size. Their chemical compositions are listed in Table I. As seen from Table I, the main compositions for cermets are TiCN, TaC and WC, and those for cemented carbides are WC, TiC and TaC. The specimen shape and dimensions are shown in Fig. 1. For cemented carbides, two specimen sizes, $8 \times 4 \times 25$ and $16 \times 4 \times 25$ mm, were prepared, but for cermets, the specimen size was $8 \times 4 \times 25$ mm. All specimens were polished with diamond paste to the mirror-like finish prior to the tests. The mechanical properties after sintering are listed in Table II. The value of fracture toughness for the cemented carbides is 12.7 $MPam^{1/2}$, a little higher than that

TABLE I Chemical compositions of the material used

	Wt (%)					
	WC	TiC	TaC	NbC	Co	
Cemented carbides	72	8	8	2	10	
	WC	TiCN	TaC	Ni	Co	Mo
Cermets	15	50	10	8	8	9

TABLE II Mechanical properties of the materials used

	Cemented carbides	Cermets
Coefficient of linear expansion	5.34×10^{-6}	7.96×10^{-6}
Young's modulus (GPa)	527.24	428.26
Poisson' modulus	0.222	0.233
K_{IC} (MPam$^{1/2}$)	12.7	10.86
Bending strength (MPa)	2600	2150

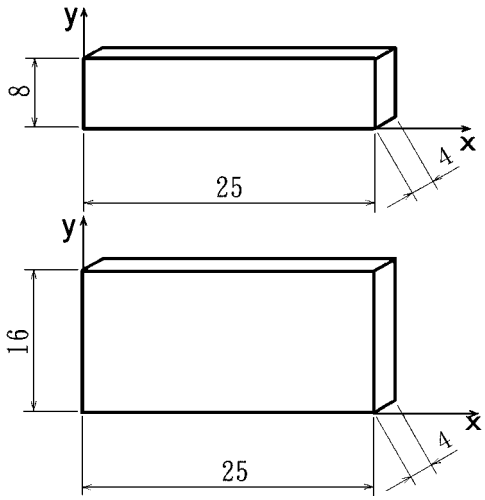

Figure 1 The shapes and dimensions of the specimens.

(= 10.86 MPam$^{1/2}$) for the cermets. A similar trend is also seen in bending strength.

2.2. Experimental procedures

2.2.1. Measurement of temperature distributions

All surfaces of the specimen but the bottom were coated with a silicone resin to provide them with adiabatic boundary conditions. The surface without coating was planned to contact the cooling media. The specimens were heated in the furnace for 20 minutes. Then the specimens were dropped down to contact the cooling media at 293 K, and left there for 5 minutes. For the cooling media, water and silicon oil were used in the present study. Their coefficients of kinematic viscosity are 0.89×10^{-6} m^{2}s^{-1} and 5×10^{-6} m^{2}s^{-1} [17], respectively.

Repeated thermal shock tests were conducted using a timer-controlled motor that can lift or lower the specimen between the furnace and the cooling medium, as shown in Fig. 2. From the preliminary experiments, temperature variations in the length and width dimensions of the specimen were confirmed as small. So, we can assume that the only dimensional temperature gradient is in the specimen height. Measurements of the temperature gradient along the specimen height were done by using five Alumel-Chromel thermocouples with 0.2 mm diameter. These were attached to the specimen's side at 0, 1, 2, 4 and 8 mm for the 8 mm high specimens, and 0, 1, 2, 4, and 16 mm for the 16 mm high specimens, (Fig. 3) measured from the cooled surface (bottom of the specimen). These temperature measurements were done five times at constant heating temperatures. The averaged temperature distributions were used for the calculations of the dynamic thermal stresses induced during the thermal shock test.

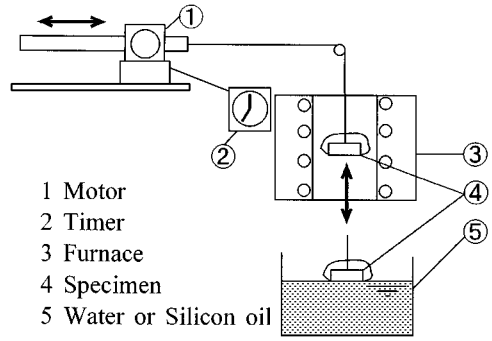

Figure 2 A schematic illustration of the thermal shock testing equipment.

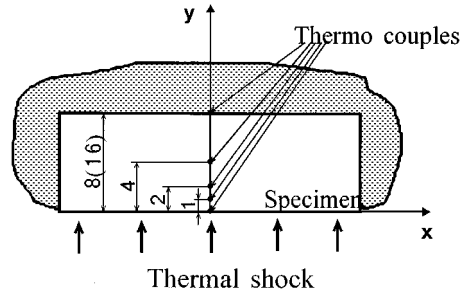

Figure 3 The locations of thermocouples attached to the specimen to measure the temperature distribution in the specimen height during the thermal shock.

2.2.2. Analysis of thermal stresses

When the temperature gradient does not occur in the longitudinal and transverse directions of the specimen but only in the direction of the specimen height, thermal stresses can be evaluated by the following expression [18],

$$\sigma_x(t, y) = -\frac{\alpha E T(t, y)}{1-\nu} + \frac{1}{2c(1-\nu)} \int_0^{2c} \alpha E T(t, y)\, dy + \frac{3y}{2c^3(1-\nu)} \int_0^{2c} \alpha E T(t, y) y\, dy \quad (1)$$

where α, E, ν denote the linear coefficient of thermal expansion, Young's modulus and Poisson's ratio of the material, respectively. In addition, 2c indicates the specimen height, and T denotes the temperature gradient. In this calculation, the variations of the thermal

and mechanical properties with temperature changes were expected to be small [19], so the averaged values in the temperature's range were employed for the calculations. The numerical integral method was used for the calculation of the above expression.

2.2.3. Crack growth behavior in the repeated thermal shock test

Precrack was introduced at the center of the specimen by the bridge indentation method. Their lengths ranged from 100 to 150 μm. The specimen surfaces containing the indentation were polished, eliminating about 40 μm, to remove the effect of residual stresses induced by the bridging indentation. Crack length during the fatigue process was measured by an optical microscope at magnification of 400∼1000 by interrupting the test at the specified number of cycles. The relationship between da/dN-K_{max} was obtained from the observed crack growth curve 2a-N.

The Newmann-Raju expression [20] for surface crack in bending was employed in the calculation of K_{max}. The crack shapes for the surface cracks were found to be b/a = 0.74, where b and a denote a crack depth and a half crack length, respectively. The smooth unnotched specimens were also tested to study the differences in the crack initiation behavior between cermets and cemented carbides during the repeated thermal shock tests.

3. Effects of specimen heights and cooling medium on the thermal shock behavior

3.1. Temperature distribution in the specimen during thermal shock

Fig. 4a and b show the temperature distribution in the direction of the specimen height at the elapsed time of 0.5 sec after thermal shock. The distribution was obtained for the case of a heating temperature of 523 K. From Fig. 4a, a small difference can be seen between the 8 and 16 mm height specimens in the temperature distributions, though a sudden temperature change near the cooled specimen surface due to thermal shock is commonly seen for both specimens. On the other hand, in Fig. 4b, which indicates the effect of the cooling medium on the temperature distributions, the temperature for the case of silicon oil changes more slowly in the direction of specimen height than in water.

3.2. Dynamic thermal stresses

The experimentally obtained temperature distributions were substituted into Equation 1 to calculate the dynamic thermal stresses induced in the specimen at the instance of the thermal shock.

Fig. 5 shows the variations of the thermal stresses with the distance from the cooled surface for several elapsed times from the beginning of the thermal shock. This figure shows the data for the case of a heating temperature of 523 K and specimen size 8 × 4 × 25 mm. As a cooling medium, water was employed. We can see that the maximum thermal stresses are always found at the

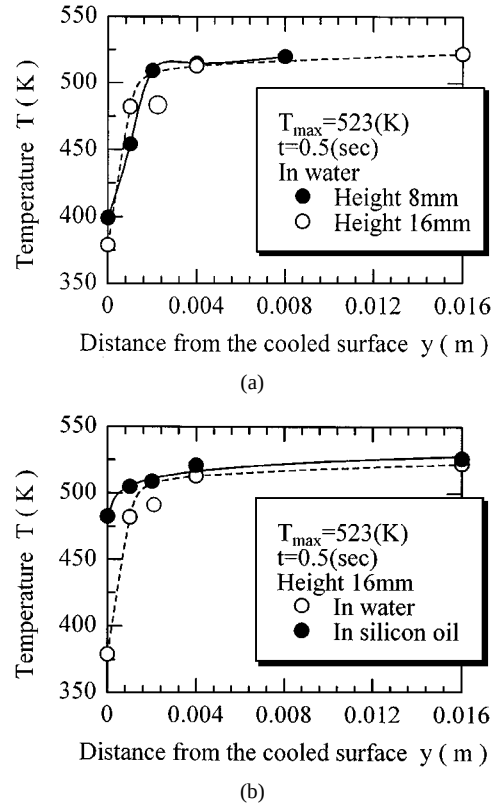

Figure 4 The effects of specimen heights and the cooling medium on the temperature distributions in the direction of the specimen height at the elapsed time of 0.5 sec. (a) Effect of the specimen height. (b) Effect of the cooling medium.

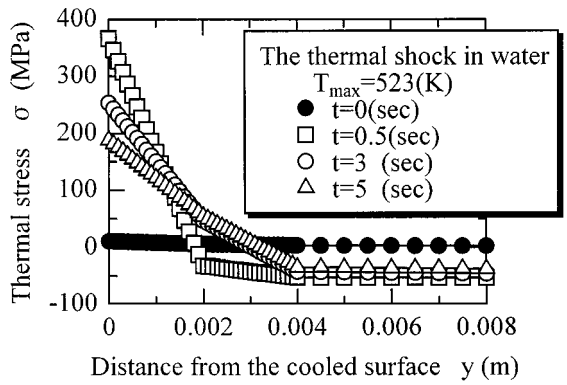

Figure 5 Distributions of the thermal stresses in the specimen induced by the thermal shock near the cooled surface with time.

cooled surface of the specimen, and they are in tension. These tendencies are common to other experimental conditions.

Fig. 6a and b show the changes in the thermal stresses, σ_{cool}, that are seen at the cooled specimen surface as a function of time for the case of the heating temperature of 523 K. From Fig. 6a, we can see that the maximum thermal stresses appear at the elapsed time of 0.5 second for both 8 and 16 mm high specimens, but the absolute values of the thermal stresses differ with the specimen height. The value for the 16 mm high specimen is 1.3 times larger than that for the 8 mm high specimen. In Fig. 6b, different behavior in the variations of the thermal stresses can be seen between water and silicon oil. The maximum stresses σ_{max} for water are at 0.5 sec, and the value is 470 MPa, while for silicon oil, it occurs at

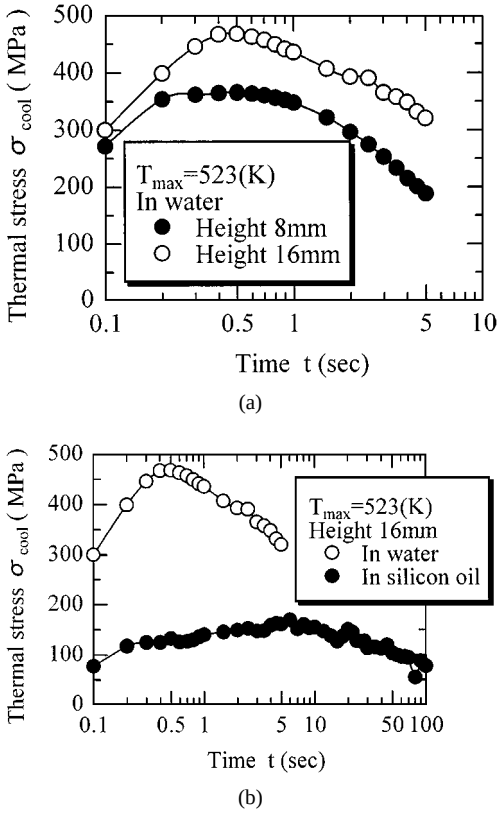

Figure 6 Variations of the thermal stresses σ_{cool} occurred at the cooled surface with elapsed time. (a) Effect of the specimen height. (b) Effect of the cooling medium.

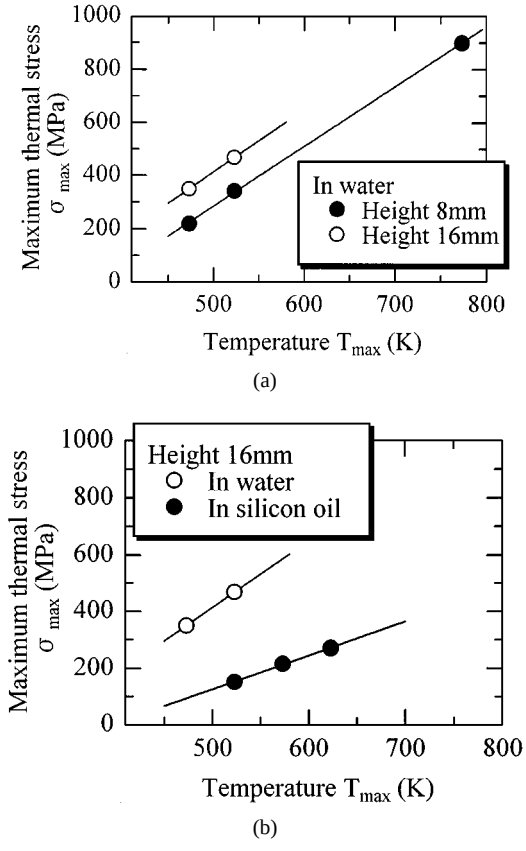

Figure 7 Changes of the maximum dynamic thermal stresses during the thermal shock as a function of the heating temperatures of the specimens. (a) Effect of the specimen height. (b) Effect of the cooling medium.

6 sec and the value is 160 MPa. So, we notice that σ_{max} for silicon oil is only 0.34 times of that for water, and changes very slowly by comparison.

Fig. 7a and b show the variations of the maximum thermal stresses σ_{max} as a function of the heating temperature T_{max} of the specimen. As seen from Fig. 7a, positive linear relationships can be seen between σ_{max} and T_{max}. At a constant T_{max}, the maximum thermal stresses for the 16 mm high specimen are larger than those for the 8 mm high specimen, though the slopes for both relations are almost same. On the other hand, in Fig. 7b indicating the effect of the cooling media, the slope of the linear relationship in silicon oil is more gentle than that in water.

3.3. Cyclic crack growth behavior in the repeated thermal shock tests

Fig. 8 shows the relationship between crack growth rate, da/dN, and stress intensity factor, K_{max}, on the log-log plot under the repeated thermal shock tests for both 8 and 16 mm high specimens. In the tests, water was used as a cooling medium. As seen from this figure, there are linear relationships between da/dN and K_{max} for both specimens besides the region of low stress intensity, and no differences exist between them. As stated above, since there is no specimen size dependence in the relationships between da/dN and K_{max}, we can realize the effectiveness of the present method to determine crack growth behavior under repeated thermal shock.

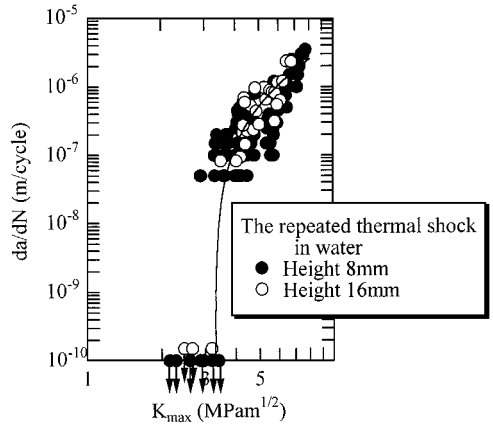

Figure 8 Effect of specimen heights on the relationship da/dN-K_{max} for the repeated thermal shock tests.

Fig. 9 shows the effect of the cooling medium on the relationships between da/dN and K_{max} under repeated thermal shock. In the tests, the specimen size $16 \times 4 \times 25$ mm was used. As seen from this figure, there are linear relationships between da/dN and K_{max} except the low stress intensity range on the log-log plot. In addition, the relationships are independent of the cooling medium employed. This fact indicates that even if the thermal boundary conditions between the specimen surface and cooling medium would be unexpected, we can evaluate the exact thermal stresses that appear along the cooled specimen surface by using the present method.

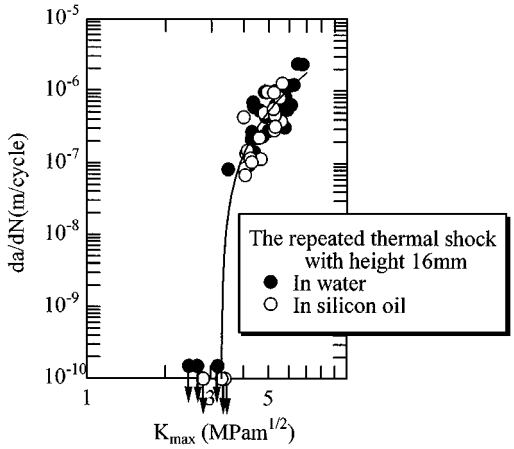

Figure 9 Effect of quenching medium on the relationship da/dN-K_{max} for the repeated thermal shock tests.

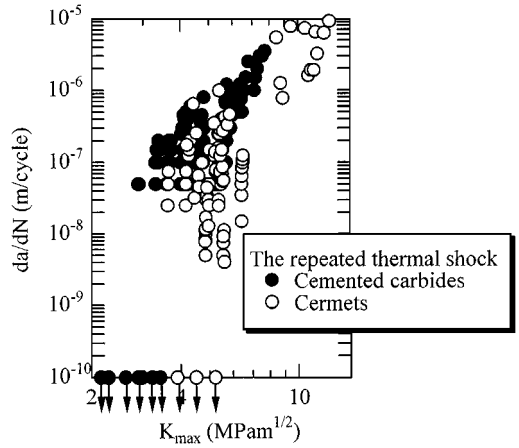

Figure 10 The relationship between da/dN and stress intensity factor for cermets and cemented carbides in the repeated thermal shock tests.

By applying the least squares method to Figs 8 and 9, we get the following intrinsic relationship between da/dN and K_{max} that is independent of the specimen size and the cooling medium:

$$da/dN = 2.02 \times 10^{-7}(K_{max} - 3.3)^{1.56} \qquad (2)$$

3.4. Estimation of thermal fracture toughness under thermal shock condition

The heating temperatures of the specimen at which precracks of size 2a begin to propagate more than 100 μm by a single thermal shock were investigated. By applying these temperatures as shown in Fig. 7a, we can estimate the dynamic thermal stresses and evaluate thermal fracture toughness values K_{IC} using the Newmann-Raju expression for surface cracks in bending. The values of K_{IC} are listed in Table III. The average fracture toughness values are estimated as 10.7 MPam$^{1/2}$ for the specimens of 8 mm height, and 9.8 MPam$^{1/2}$ for the 16 mm specimens. Though the value for the former is somewhat higher than for the latter, they are considered to be almost the same. But these estimated values are smaller than those obtaining by the bridge indentation method listed in Table II. One of the reasons for this difference is expected to be oxidization of the specimen under high temperature, but the details of the mechanisms are unknown at the present.

TABLE III The values of fracture toughness obtained by the present method

T_c (K)	σ_{max} (MPa)	2a (μm)	K_{IC} (MPam$^{1/2}$)
(a) Specimen height 8 mm			
586	479.14	836	10.98
607	526.39	358.175	7.83
613	539.89	538.175	9.86
685	701.89	710	14.77
699	733.393	306.35	10.1
			Aver. 10.71
(b) Specimen height 16 mm			
586	705.2	321.3	9.97
633	861.05	162.8	8.66
648	910.76	230.45	10.9
			Aver. 9.84

4. Repeated thermal shock behavior for cermets and cemented carbides

4.1. Crack growth behavior

Fig. 10 shows the differences in crack growth behavior under repeated thermal shock between cermets and cemented carbides. As seen from this figure, in the low stress intensity factor region, we can see that crack growth rates for cemented carbides are faster than those for cermets. In the high stress intensity factor region, there is little difference in the crack growth rates for both materials. In addition, the slope of cermets in the relation is steeper than that of cemented carbides. This result suggests a more brittle manner crack growth behavior in cermets than in cemented carbides.

4.2. Crack initiation behavior on the unnotched smooth specimen during repeated thermal shock

Crack initiation behavior for both cermets and cemented carbides were studied on the unnotched smooth specimen during repeated thermal shock tests. Many visible small cracks were initiated at the interfaces between hard phases and binder phases by the thermal shocks. The number of cracks increased with the number of thermal shocks applied. By coalescences among these small cracks, a large macroscopic crack appeared and propagated catastrophically.

Fig. 11 shows variations of the number of cycles to crack initiation Ni as a function of the maximum thermal stresses during thermal shock excursion. The data plotted at 0.5 cycles indicate bending strength [3–4]. As seen from this figure, the number of cycles to macrocrack initiation for cemented carbides is larger than those of cermets in the high stress region, while in the low stress region, the reverse trend is seen.

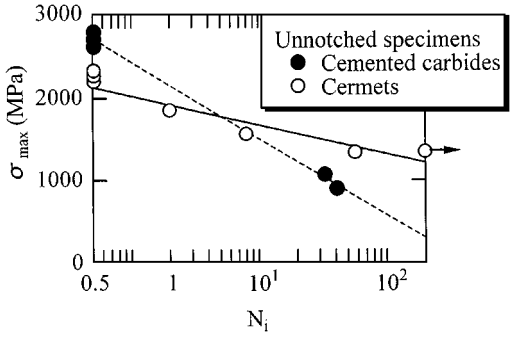

Figure 11 The relationship between maximum thermal stresses and number of cycles to crack initiation observed with unnotched smooth specimen.

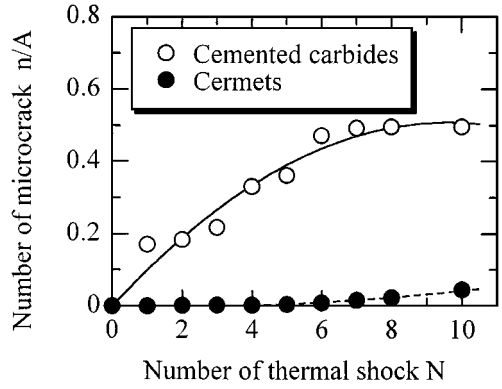

Figure 13 Variations of number of cracks per area with number of thermal shocks.

4.3. Observations of microcracks initiated during thermal fatigue process

We investigated the changes in the microstructures of the materials and crack growth morphology during the repeated thermal shocks to clarify the differences in thermal shock behavior for both materials.

Fig. 12 shows the microstructures of cermets and cemented carbides before applying thermal shocks and after applying five thermal shocks. In cemented carbides, many microcracks initiate at the interface between the matrix and binder phases as shown by arrows in this figure. In cermets, however, few microcracks are initiated even after receiving five thermal shocks. The crack paths observed in cemented carbides chiefly consist of the interfaces between the matrix and binder phases, and the interior in the binder phases. So cracks in cemented carbides propagate in an enhanced zigzag manner. On the other hand, in cermets, cracks propagate in a less zigzag manner than in cemented carbides, perhaps due to its smaller microstructural size.

Fig. 13 shows the variations of the crack densities with numbers of the thermal shocks for both cermets and cemented carbides. In cemented carbides, the number of cracks per area increases monotonically with increasing numbers of thermal shocks. In cermets, no

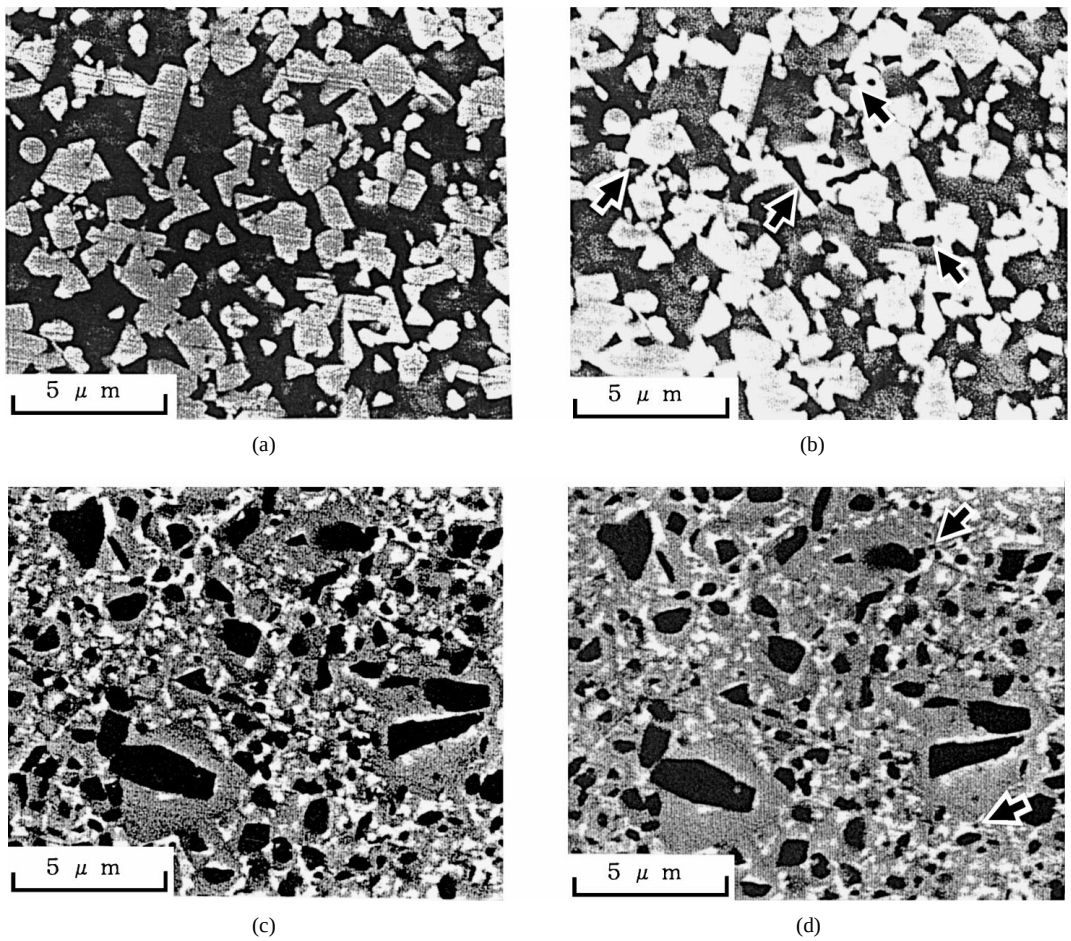

Figure 12 Appearances in the microstructures before and after thermal shocks for cermets and cemented carbides. (a) Cemented carbides before thermal shock. (b) Cemented carbides after thermal shock. (c) Cermets before thermal shock. (d) Cermets after thermal shock.

crack initiations were confirmed within 10 cycles. The above results indicate a big difference in the nucleation behavior of microcracks for cermets and cemented carbides.

4.4. On the differences in the crack growth behavior between cermets and cemented carbides under repeated thermal shocks

We can consider cermets and cemented carbides as hybrid materials which are composed of a ductile binder phase and a hardened brittle phase. The hardened brittle phases are TiCN and WC for cermets and cemented carbides, respectively, and the ductile binder phases are Ni and Co for cermets and Co for cemented carbides.

In cemented carbides, the coefficients of linear expansion for the hardened phase (WC) and the binder (Co) are $3.84 \times 10^{-6}\,K^{-1}$ and $12.3 \times 10^{-6}\,K^{-1}$, respectively. In cemented carbides, because the difference in the coefficient of linear expansion between the two is rather large and the value of Young's modulus is also large (696 GPa), thermal stresses become fairly large and cause microcracks at the interface between WC and Co as shown in Fig. 12. On the other hand, in cermets, the coefficient of linear expansion for the hardened phase (TiC or TiN) and the binder phase (Ni or Co) are $9.35 \times 10^{-6}\,K^{-1}$ and $13.3 \times 10^{-6}\,K^{-1}$, respectively. As the difference between these values and Young's modulus (215–451 GPa) are not large, it is considered that thermal stresses are not sufficient to initiate thermal cracks in cermets.

In cemented carbides, the microcracks should cause crack acceleration by coalescences between the microcracks and the main crack, especially at low stress intensity factor or low heating temperature of the specimen. At high stress intensity factor, too many microcracks are initiated, and cause crack deceleration by the interactions between them. Cracks are thought to propagate by avoiding the hard phase. So, in cemented carbides, cracks are deflected because the sizes of the hard phase such as WC are large as compared with those in cermets. This enhanced crack deflection in cemented carbides is also the reason for a steady subcritical crack growth behavior for this material by reducing the mode I component and increasing the mode II component of the stress intensity factor.

In cermets, the number of cracks that initiate during thermal shock at low heating temperature is not large enough to cause crack acceleration. This is the reason for the high crack resistance of cermets at low stress intensity range. But at high stress intensity range, it is expected that cracks should propagate in a more brittle manner than in cemented carbides because of its less crack-deflecting morphology.

As seen in Fig. 11, at the low thermal stress region where subcritical crack growth is dominating fatigue lives, the fatigue lives for cermets become longer than those for cemented carbides, since cermet shows a higher resistance to crack initiations and propagation at low stress intensity than cemented carbides.

5. Conclusions

The following results were reached in the present study.

1. The relationships between da/dN and stress intensity factor, K_{max}, and the values of fracture toughness under repeated thermal shocks were studied using the new testing method. We confirmed that the relationships are independent of specimen sizes and the cooling medium employed. The following intrinsic expression for the da/dN and K_{max} was obtained for cemented carbides:

$$da/dN = 2.02 \times 10^{-7}(K_{max} - 3.3)^{1.56}$$

2. The values of fracture toughness determined by the present method are independent of specimen sizes, but are lower than those estimated by the bridging indentation method. The reason for this is unclear at present, but some oxidization effects in the high temperature environment are expected.

3. Cermets and cemented carbides were studied under repeated thermal shock to obtain the relationships between da/dN and K_{max} using the new testing method. At low stress intensity factor, crack growth rates for cemented carbides are faster than those for cermets, but no differences between them were observed at high stress intensity factor. The above differences at the low stress intensity for both materials was thought to be due to the differences in the coefficients of linear expansion between the hard phase and the binder phase.

4. Variations of the number of cycles to crack initiation N_i as a function of the maximum thermal stresses were investigated on the unnotched smooth specimen during repeated thermal shocks. At low stress, or in the long life region, thermal fatigue strength for cermets exceeded those for cemented carbides.

References

1. Y. IYORI, N. SIMA and H. IDA, *Technological report of Hitachi Kinzoku* **5** (1987) 65.
2. S. ISHIHARA, T. GOSHIMA, K. MIYAO, T. YOSHIMOTO and S. TAKEHARA, *Trans. Jpn. Soc. Mech. Eng.* **57-536** A(1991) 824.
3. S. ISHIHARA, T. GOSHIMA and K. MIYAO, *Trans. Jpn. Soc. Mech. Eng.* **57-543** A(1991) 2735.
4. S. ISHIHARA, T. GOSHIMA, K. MIYAO, T. YOSHIMOTO and S. TAKEHANA, *JSME Int. J. Ser.* **I 34-316** A(1991) 490.
5. T. NISHIKAWA, T. GAO and M. TAKATSU, *J. Soc. Mat. Sci. Japan* **42-476** (1993) 507.
6. H. ABE, N. YOKOTA, Y. SATOO and Y. FUKUDA, *J. Soc. Mat. Sci. Japan* **42-482** (1993) 1312.
7. H. ABE and N. YOKOTA, *Trans. Jpn. Soc. Mech. Eng.* **60-578** A(1994) 2207.
8. M. KUBOUCHI and H. HOJO, *J. Soc. Mat. Sci. Japan* **39-437** (1990) 202.
9. T. NISHIKAWA, T. GAO, M. KOSAKAI, T. NISHIBE and M. TAKATSU, *J. Soc. Mat. Sci. Japan* **41-464** (1992) 561.
10. T. SAKUMA, U. IWATA and H. TAKAKU, *Trans. Jpn. Soc. Mech. Eng.* **58-547** A(1992) 470.
11. T. SAKUMA, U. IWATA and H. TAKAKU, *Trans. Jpn. Soc. Mech. Eng.* **58-552** A(1992) 1424.
12. K. NIIHARA, J. P. SINGH and D. P. H. HASSELMAN, *J. Mater. Sci.* **17** (1982) 2553.
13. J. P. SINGH, Y. TREE and D. P. H. HASSELMAN, *J. Mater. Sci.* **16** (1981) 2109.

14. P. F. BECHER, D. LEWIS III, K. R. CARMAN and A. C. GONZALEZ, *Ceramic Bulletin* **59** (1980) 542.
15. S. ISHIHARA, T. GOSHIMA, I. NAKAYAMA and T. YOSHIMOTO, Proc. 1st Int. Symp. Thermal Stresser '95 Hamamatsu (1995) 147.
16. S. ISHIHARA, T. GOSHIMA, I. NAKAYAMA and T. YOSHIMOTO, *Trans. Jpn. Soc. Mech. Eng.* **62-598** A(1996-6) 1327.
17. "Thermophysical Properties Handbook" (Youkendou, 1990) p. 34.
18. Y. TAKEUTI, "Analyses of Thermal Stresses" (Nisshin, 1989) p. 13.
19. K. SHINOHARA, F. UETA and T. TANASE, *J. Jpn. Soc. Powder and Powder Metallurgy* **40-1** (1993) 29.
20. J. C. NEWMAN JR. and I. S. RAJU, NASA TP-1578 (1979).

Received 18 February 1997
and accepted 20 August 1998